Supporting Information:

Ion channels made from a single

membrane-spanning DNA duplex

Kerstin Göpfrich,[†] Chen-Yu Li,[‡] Iwona Mames,[¶] Satya Prathyusha

Bhamidimarri,[§] Maria Ricci,[†] Jejoong Yoo,[‡] Adam Mames,[¶] Alexander

Ohmann,[†] Mathias Winterhalter,[§] Eugen Stulz,*,[¶] Aleksei Aksimentiev,*,[‡] and

Ulrich F. Keyser *,[†]

[†]*Cavendish Laboratory, University of Cambridge, Cambridge CB3 0HE, United Kingdom*

[‡]*Center for the Physics of Living Cells, Department of Physics, University of Illinois at*

UrbanaChampaign, 1110 West Green Street, Urbana, Illinois 61801, United States

[¶]*School of Chemistry & Institute for Life Sciences, University of Southampton, Highfield,*

Southampton SO17 1BJ, United Kingdom

[§]*Jacobs University Bremen, 28759 Bremen, Germany*

E-mail: est@soton.ac.uk; aksiment@illinois.edu; ufk20@cam.ac.uk

Phone: +44(0)238059 9369; +1(0) 217333 6495; +44(0)1223 337272

Contents

1. Materials and Methods

1.1 Note S1: Design and synthesis of the porphyrin-tagged duplex.

Design of the duplex. The DNA sequences of the porphyrin-tagged duplex are shown in Figure 1B (main paper). Each 25-mer ssDNA contains three porphyrins, which form a stacked array upon hybridization *(4)*. In the assembled dsDNA, an 8-nt overhang persists which is located outside the lipid bilayer in order to orient the dsDNA in an orthogonal manner to the lipid bilayer and may be used as additional anchor.

Synthesis of the porphyrin monomers. The modified monomers were obtained according to procedures described previously *(4)*. Following this protocol the porphyrins were transformed into the DMT-protected nucleosides. The first porphyrin with the acetylene (rigid) linker (labelled "1" in Figure 1B, main paper) was obtained *via* Sonogashira coupling (Figure S1 A), and the second porphyrin containing a flexible linker (labelled "2" in Figure 1B, main paper) was obtained through coupling of the monocarboxylic acid functionalized porphyrin with the propargylamine derivative of 5-iodo-2'-deoxyuridine (Figure S1 B). The building blocks were phosphorylated and used immediately in solid phase DNA synthesis.

Synthesis and purification of the porphyrin oligonucleotides. The porphyrin oligonucleotides were synthesized using an Applied Biosystem Expedite synthesizer on solid phase support (SPS; Glen Research, pore size: 1000 Å) on a 1.0 µmol scale, using standard phorphoramidite chemistry. The unmodified nucleotides and reagents were obtained from Cambio, UK, or Tides Service Technology, Germany. For the porphyrin nucleosides, an extended coupling time of 6 minutes was used. Optionally, the DNA was additionally functionalized with a biotin at the 5'-end using standard procedures for future modification.

The purification of modified DNA was carried out by RP-HPLC using a Waters XBridge OST C18, 2.5 µm 4.6 x 55 mm² column; flow rates were set to 1 mL/min; gradient and eluents used for separation of DNA are described in Table S1. The concentration of the DNA was determined from the optical absorbance at 260 nm by UV spectroscopy *(5)*. For some experiments, the DNA oligomers were treated with tetra butyl ammonium (Sigma Aldrich).

1.2 Note S2: Atomic force microscopy.

For sample preparation, the mica disks (9.9 mm diameter, Agar Scientific, Stansted, Essex, UK) were attached on metallic disks (AFM Stainless Steel Disks, SPI Supplies, West Chester, Pennsylvania, USA) with epoxy glue (Araldite rapid 2 x 15 mL, Araldite professional adhesives, Basel, Switzerland). 5 µL of the sample solutions in 10 mM Tris-HCl, 1 mM EDTA, 20 mM $MgCl_2$, pH 8.0 were deposited on the freshly cleaved mica surface and incubated for 90 seconds. The concentration of the duplex was 5 µM. Subsequently the surface was rinsed with 3 mL of Milli-Q water (Merck Millipore, Billerica, Massachusetts, USA) to remove the excess of sample and blow-dried with nitrogen. Finally the samples were placed on the atomic force microscope sample stage.

Imaging was carried out on a commercial Cypher S AFM (Oxford Instrument, Asylum Research, Santa Barbara, California, USA). The imaging process was performed in amplitude modulation in air and at room temperature using AC240TS cantilevers (Olympus, Tokyo, Japan) with a nominal spring constant of 2 N/m. The set-point to free amplitude ratio was

generally kept around to 70 % with a free oscillation amplitude of 20 nm. The frequency of excitation was set close to the resonance of the first flexural mode (around 70 kHz) and a repulsive mode was preferred. The scan speed was set to either 1 or 2 Hz obtaining an image of 256 x 256 pixels with different magnifications. The images were flattened and band-pass filtered using Gwyddion – free SPM data analysis software (http://gwyddion.net/).

1.3 Note S3: Lipid vesicle preparation.

1,2-Diphytanoyl-sn-glycero-3-phosphatidylcholine (DphPC; Avanti Polar Lipids, AL), 10 % cholesterol (Avanti Polar Lipids) giant unilamellar vesicles (GUVs) were prepared via electroformation using the Vesicle Prep Pro unit (Nanion technologies, Germany) and a protocol adapted from Ref. *(6)*. DphPC lipids were dissolved in chloroform to a final concentration of 50 mg/mL and mixed with cholesterol (10 % by weight). A 20 µL droplet of this solution was spread evenly on each of two indium tin oxide-coated glass slides (VisionTek Systems, Ltd., UK), which were placed in the electroformation unit and filled with 1 M sorbitol. An AC-current (3 V_{p-p}, 5 Hz) was applied for 2 hours. GUVs were stored at 4 °C for up to a week.

1.4 Note S4: Confocal fluorescent imaging.

For confocal imaging, we took advantage of the fluorescent properties of porphyrin itself. A porphyrin-free Cy3-tagged duplex (Integrated DNA Technologies) served as a control. Vesicles were suspended in 500 mM KCl, 10 mM MES, pH 6.0 in an incubation chamber (Grace Biolabs) and imaged using a Confocal Leica TCS SP5 microscope with a 60x oil immersion objective in bright field and fluorescence mode. While imaging, the duplex was added at a concentration of 5 nM. Porphyrin and Cy3 were excited at 514 nm using an argon and a HeNe594 laser and emission was collected above 530 nm. Images were processed using ImageJ.

1.5 Note S5: Ionic current recordings.

Ionic current recordings were carried out using solvent (n-decane, Alexis) containing DphPC membranes *(7)* (Avanti Polar Lipids) following the detailed protocol by Gutsmann et al. *(8)*. Solvent containing membranes are known to promote pore insertion and have previously been used for the discovery of new protein pores *(8)*. Current data was acquired at a sampling rate of 1 kHz using an Axopatch 200B amplifier and analysed in Matlab and Clampfit. After a stable membrane was formed, the duplex was added to the *cis* side at concentrations between 1 and 3 nM in 1 M KCl, 10 mM MES, pH 6.0.

1.6 Note S6: Molecular dynamics simulations.

General MD methods. All molecular dynamics simulations were performed using the program NAMD2 *(9),* periodic boundary conditions, the CHARMM36 parameter set for

4

water, ions and nucleic acids *(10),* CHARMM parameters for the DphPC lipid bilayer *(11),* custom parameterization of ion-DNA and ion-ion interactions *(12).*

All simulations employed a 2-2-6 fs multiple time stepping, SETTLE algorithm to keep water molecules rigid *(13),* RATTLE algorithm to keep all other covalent bonds involving hydrogen atoms rigid *(14),* a 8-10-12 Å cut-off for van-der-Waals and short-range electrostatic forces. Long-range electrostatic interactions were computed using the particle mesh Ewald (PME) method *(15)* over a 1.2 Å resolution grid *(16).*

Assembly of the simulation system. The duplex was converted to idealized all-atom structures using a previously described method *(17).* To describe the porphyrin groups covalently attached to the DNA, chemical models, including all atoms of the linkers, were created; force field parameters were obtained using the CHARMM General Force Field (CGenFF) webserver. Matching the experimental design of the DNA duplex, porphyrin groups were added to DNA via custom patches in the conformation suggested by the previous structural model *(4).*

The DphPC lipid membranes were prepared by replicating a small patch of a pre-equilibrated lipid bilayer *(18).* After merging the duplex with the DphPC lipid membrane, DphPC molecules located either within 3 Å of the channel or inside the channel were removed. Mg^{2+}-hexahydrates *(12)* were randomly placed near the channels in the amount required to exactly compensate the electrical charge of the latter. Following that, water and 1 M KCl were added using the Solvate and Autoionize plugins of VMD.

Equilibration of the all-atom models. Upon assembly, the duplex system was minimized using the conjugate gradient method for 1200 steps to remove steric clashes.

During the minimization process, all non-hydrogen atoms of the duplex were harmonically restrained (with the spring constant k_{spring} = 1 kcal/(mol Å^2)) to their initial coordinates. After minimization, the duplex system was equilibrated under the NPT condition, where the number of atoms (N), pressure (P) and temperature (T) were kept constant. The pressure was set to 1 atm using the Nosé-Hoover Langevin piston method *(19,20).* The temperature was maintained at 295 K using a Langevin thermostat *(21).*

The ratio of the system's dimensions along the x and y axis were constrained while the *z*-axis was decoupled. In the first step of the equilibration protocol, the duplex system was simulated for 48 ns with all non-hydrogen atoms of the duplex harmonically restrained (with the spring constant k_{spring} = 1 kcal/(mol Å^2)) to their initial coordinates, allowing the lipid and water to equilibrate around the channel.

In the second step, spatial restraints were replaced by a network of harmonic restraints that maintained distances between atomic pairs at their initial values; such elastic restraints excluded hydrogen atoms, phosphate groups, atoms in the same nucleotide and pairs separated by more than 8 Å. The duplex system was simulated under such elastic restraints for 14.4 ns; the spring constants of the restraints were decreased from 0.5 to 0.1 and then to 0.01 kcal/(mol Å^2) every 4.8 ns. In the last step, the duplex system was simulated without any restraints for 137.6 ns. During all MD simulations of the DNA duplex system, the system's coordinates were recorded every 2.4 ps.

MD simulation of ionic current. All simulations of the ionic current were performed in the constant number of atom, volume and temperature ensemble. A voltage drop (*V*) across

the system was produced by applying an external electric field E such that $V = -EL$, where L was the length of the simulation system in the direction of the applied field *(22)*.

Ionic current calculations. Prior to calculations of the ionic current, frames of the MD trajectory were aligned *(22)* using a two-step process. First, we shifted the x and y coordinates of all atoms in the simulation system by the same amount to maintain the centre of mass coordinate of the duplex constant within the plane of the lipid bilayer. Next, the z-coordinates of all atoms in the system were shifted by the same amount to maintain the z-coordinate of the lipid bilayer centre of mass constant. To reduce thermal noise originating from stochastic displacements of ions in the bulk solution, the ionic current calculations were carried out within the $l/2 \leq z \leq l/2$ region of the system, where $l = 30$ Å. The instantaneous current was computed as

$$I(t + \frac{\Delta t}{2}) = \frac{1}{\Delta t\, \ell} \sum_i^N q_i(\zeta_i(t + \Delta t) - \zeta_i(t))$$ (1)

where

$$\zeta_i(t) = \begin{cases} z_i(t), & |z_i(t)| \leq \ell/2 \\ -\ell/2, & z_i(t) < -\ell/2 \\ \ell/2, & z_i(t) > \ell/2, \end{cases}$$ (2)

the sum over i indicates a sum over all ions, Δt is the time interval between two consecutive frames of the MD trajectory and q_i is the charge of ion i *(23)*. The average current of a trajectory was computed by summing up all instantaneous currents and dividing by the number of coordinate frames of the trajectory. To estimate the error, the ionic current trace was first block averaged with block size 9.6 ns. The reported standard errors of the mean were calculated from the block-averaged current traces.

Calculations of the local density and local ionic current flux. The local density and the local ionic current flux were computed as described previously *(24)*. We divided the simulation system into 5 Å x 5 Å x 5 Å grids and calculated the average density of the selected atom groups and average flux of each ion species in each grid using a sampling frequency of 240 ps. The local current in each grid in a given direction (x, y or z) was calculated by

$$I_j = \sum_i q_i \times f_{i,j}, (i = K^+, Cl^-, Mg^{2+}; j = x, y, z)$$ (3)

where i is the ion species (K^+, Cl^- or Mg^{2+}), q_i is the charge of the ion and $f_{i,j}$ is the flux of the ion in the given direction. We averaged the 3-dimensional density and flux data in the cylindrical coordinate over the azimuthal angle to obtain the mean density and mean flux on the r - z plane as described previously *(25)*. Following that, the 2D density and flux were

made symmetric about the *z* axis by making a mirror image (*r* to *-r*). Finally, we used the contourf and streamplot function in the python matplotlib package to generate the local density and flux plots, which were then assembled into the final figures.

2. Structure and characterisation of the duplex
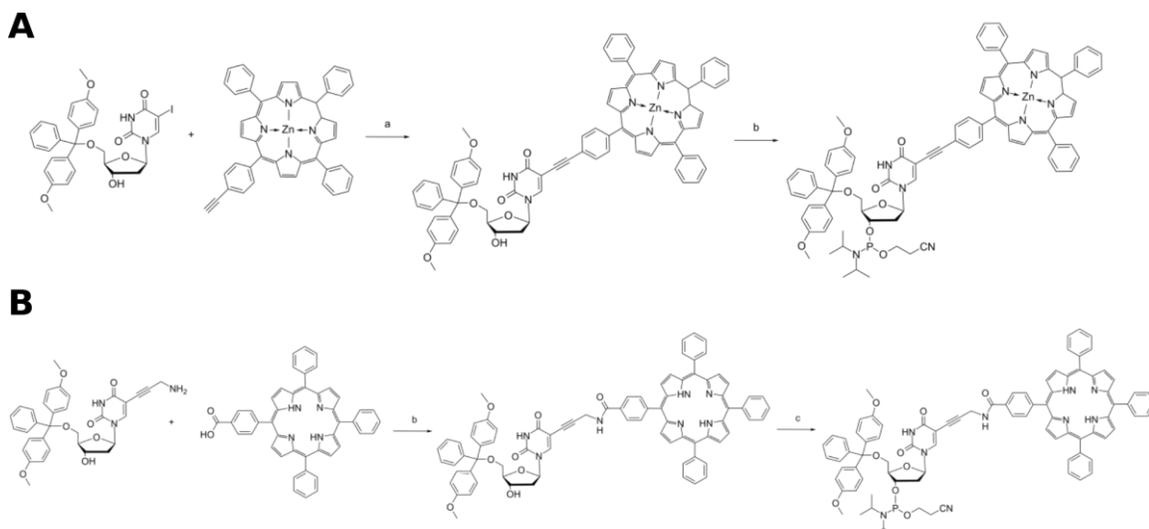
2.1. Synthesis of the porphyrin nucleotides

A

B

Figure S1. A) Synthesis of the porphyrin nucleotide with acetylene linker. Reagents and conditions: a. Pd(PPh$_3$)$_4$, CuI, Et$_3$N, DMF, rt. 70 % ; b. CEP-Cl, DIEA, DCM, rt. 90%. B) Synthesis of the porphyrin nucleotide with amide linker. Regents and conditions: b. HATU, DIPEA, DMF, rt. 78 %; c. CEP-Cl, DIEA, DCM, rt. 90%.

2.2. HPLC-traces of the porphyrin nucleotides

Table S1. Gradients and eluents used for RP-HPLC separation of the porphyrin DNA. Eluent A: 8.6 mM TEA / 100 mM hexafluoro-isopropanol − TEA buffer pH 7.5; Eluent B: methanol.

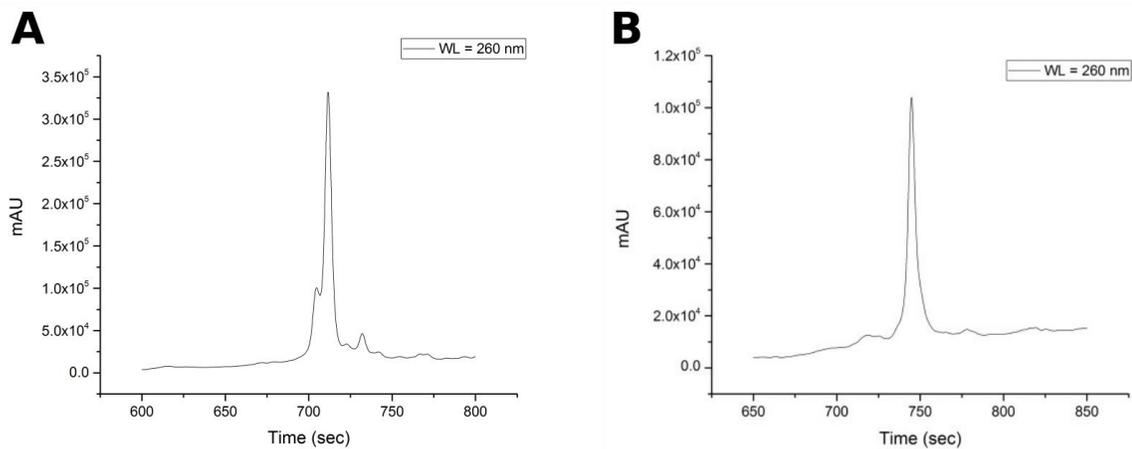| T (min)	A (%)	B (%)
0	100	
10	30	70
15	10	90
20		100
25		100
35	100	
45	100	

Figure S2. A) Trityl-off analatical RP-HPLC trace of the purified 3P−Acetylene DNA. B) Trityl-off analatical RP-HPLC trace of the purified 3P−Amide DNA.

3. Experimental results of ionic current recordings

3.1. Note S7, S8: Considerations and control experiments

Note S7: Control experiments with other DNA duplex designs.

To elucidate the design principles required to obtain a transmembrane current inducing DNA duplex, we tested two additional designs, both using the same sequence as our porphyrin tagged duplex without the single-stranded overhangs. Control 1: A duplex with a terminal cholesterol tag on the 3' end of the DNA strand with the acetylene-linker. Control 2: A duplex with two terminal cholesterol tags, one on each 3' end. Figure S3 shows example traces illustrating the outcome of these control experiments.
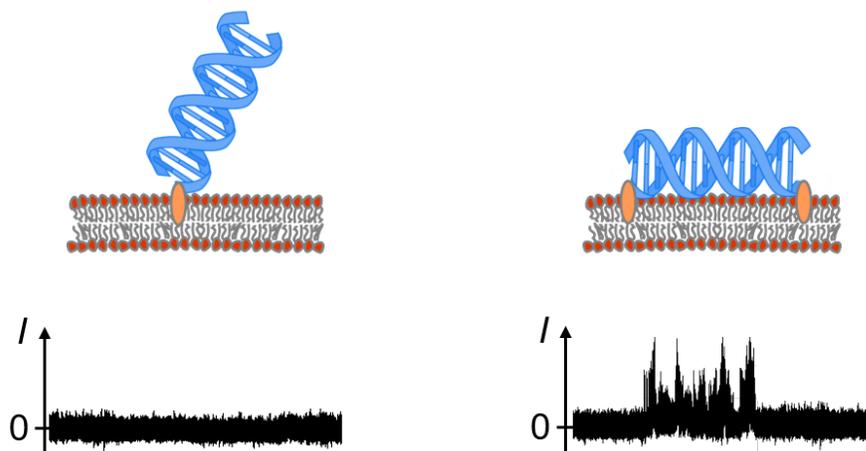

Figure S3. Control 1 (left) does not induce any transmembrane currents. Control 2 (right) causes occasional current bursts, but no stable transmembrane currents. Confocal imaging confirms that both constructs do, however, attach to the lipid membrane (data not shown).

Note S8: Clustering of porphyrin-tagged DNA.

Porphyrin-DNA has previously been shown to form distinct clusters in aqueous solutions through porphyrin stacking. This, however, has been suppressed by addition of organic solvents, thus is not expected to happen within the hydrophobic lipid bilayer environment *(4, 27)*. In addition, the duplex-induced transmembrane currents were smaller than the currents for the four-helix pore *(28)*. This suggests that we measure ion flow through toroidal pores at the lipid-DNA interface, rather than clusters forming a physical pore.

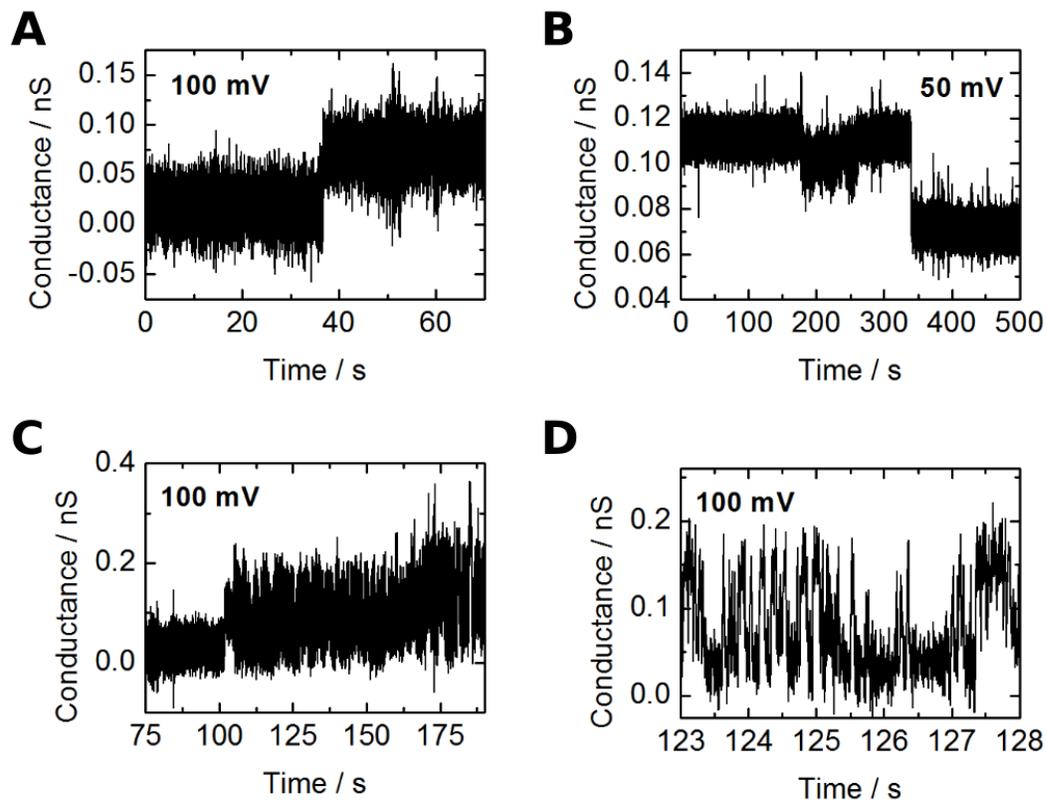## 3.2. Additional ionic current traces

Figure S4. Additional ionic current traces of the DLC recorded at 1 kHz sampling rate in 1 M KCl, 10 mM MES, pH 6.0. A) Single insertion. B) Two consecutive closure steps. The stepwise reduction in ionic conductance could be caused by duplexes flipping out of the membrane. C) Insertion of a fluctuating duplex. D) Zoom into the trace from (C).
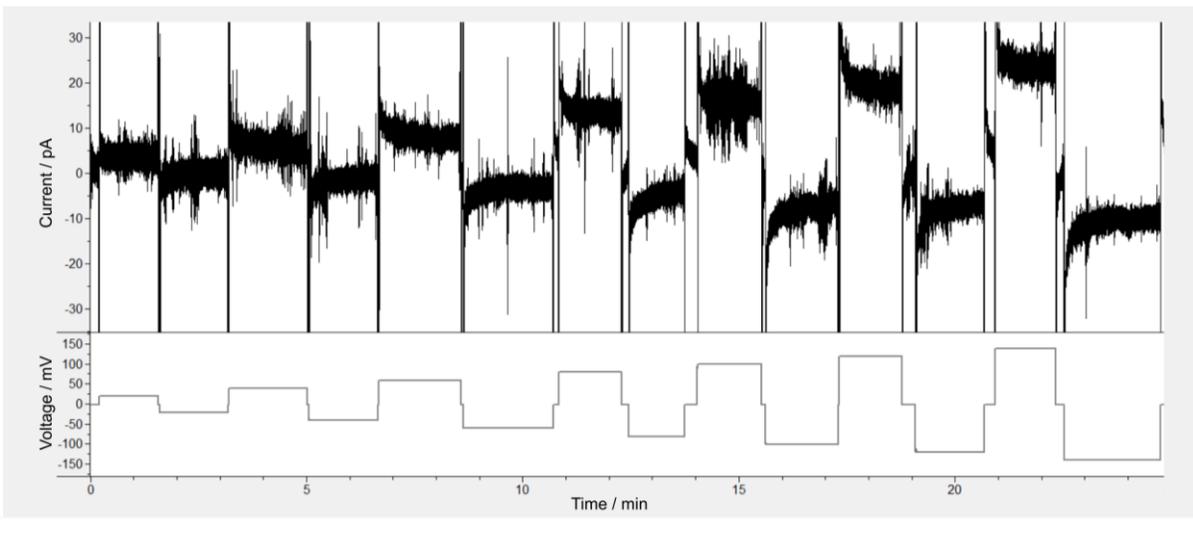
Figure S5. Exemplary IV-trace of the DLC recorded at 1 kHz in 1 M KCl, 10 mM MES, pH 6.0. All IV-curves were recorded after a clear insertion step was observed. The DLC remained stable for minutes across the voltage range between ±140mV.

4. Molecular dynamics simulation results

4.1. Equilibration of the DNA duplex – lipid bilayer interface.
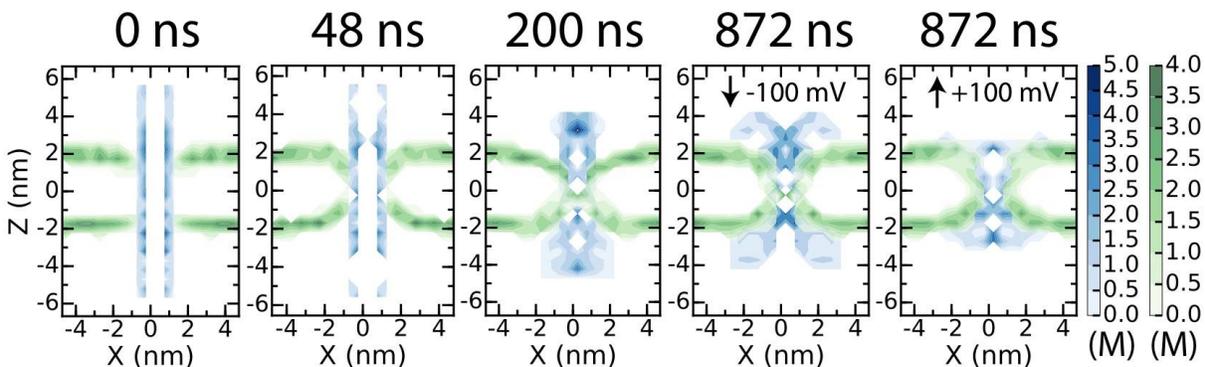

Figure S6. Local density of lipid head groups (phosphorus atoms, green) and DNA (phosphorus atoms, blue) at several stages of the MD simulation. From left to right, the snapshots illustrate the state of the system prior to equilibration (0 ns), at the end of equilibration performed having all heavy atoms of the DNA duplex restrained to their initial coordinates (48 ns), at the end of the unrestrained equilibration simulation (200 ns), and at the end of the simulations performed under -100 mV (872 ns, dark blue trace in Figure 4C) and +100 mV (872 ns, orange trace in Figure 4C) transmembrane bias. In the right two panels, the black arrow indicates the direction of the transmembrane bias. Each snapshot was computed by averaging the atomic coordinates over a short (2 ns) fragment of the 2.4-ps sampled trajectory nearest to the point of interest. To increase accuracy, the density maps were radially averaged about the z-axis (which passes through the center of mass of the duplex).
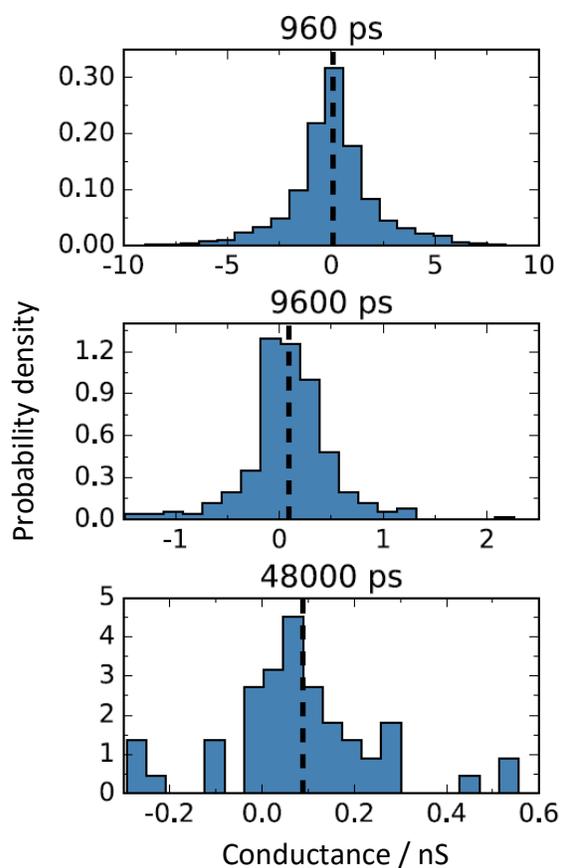
4.2. Conductance histograms

Figure S7. Normalized histograms of ionic conductance in MD simulations of the DLC. The conductance histograms were obtained by splitting the ionic current traces at +100, +30, -30, and -100 mV into blocked of specified duration, averaging the currents within each block, dividing the average current in each block by the transmembrane bias and concatenating the resulting conductance values into one data set. In each column, the histograms differ by the size of the blocks the currents were averaged over; the block size is specified at the top of each graph. The dashed lines indicate the mean conductance values. Note the different in the scale of the horizontal axes. The dependence of the ionic current histograms on the sampling rate of the simulated ionic current is discussed in detail in *(29)*. Note that the sampling rate does not influence the average value.

4.3. Note S9: Caption for Movie S1

Molecular dynamics simulation of the DNA duplex in a lipid bilayer membrane. The DNA strands are coloured in blue and yellow; the porphyrin groups are coloured in grey. The lipid molecules are drawn as lines; C, N, O and P atoms are coloured in green, blue, red and ochre, respectively. The hydrogen atoms of lipid molecules are not shown. For clarity, lipid molecules facing the viewer are removed. The slide bar at the upper right corner indicates the progression of the trajectory in nanosecond (ns). The first 200 ns of the simulation correspond to equilibration (no applied bias); the remaining part of the movie illustrates a trajectory at +100 mV bias. At the beginning of the movie, a static image illustrates the initial placement of the DNA duplex within the lipid membrane, highlighting the location of the porphyrin groups. The second stage of the movie illustrates the stochastic displacements of waters molecules around the duplex; O and H atoms of water are shown as red and white spheres, respectively. The final part of the movie illustrates the transmembrane transports. All lipid molecules are hidden; the volume occupied by water is represented by a semi-transparent surface; potassium ions are shown as green spheres. For clarity, only those potassium ions that showed considerable displacement across the lipid bilayer (top 10%) are shown.

References

1. S. M. Douglas, *et al., Nature* **459**, 414 (2009).

2. N. A. W. Bell, *et al., Nano Lett.* **12**, 512 (2012).

3. S. Hernández-Ainsa, *et al., ACS Nano* **7**, 6024 (2013).

4. A. Brewer, G. Siligardi, C. Neylon, E. Stulz, *Org. Biomol. Chem.* **9**, 777 (2011).

5. L. A. Fendt, I. Bouamaied, S. Thöni, N. Amiot, E. Stulz, *J. Am. Chem. Soc.* **129**, 15319 (2007).

6. M. I. Angelova, D. S. Dimitrov, *Faraday Discuss. Chem. Soc*. **81**, 303 (1986).

7. P. Mueller, D. O. Rudin, H. T. Tien, W. C. Wescott, *Nature* **194**, 979 (1962).

8. T. Gutsmann, T. Heimburg, U. F. Keyser, K. R. Mahendran, M. Winterhalter, *Nat. Protoc*. **10**, 188 (2015).

9. J. C. Phillips, *et al., J. Comput. Chem.* **26**, 1781 (2005).

10. A. D. MacKerell, Jr., *et al., J. Phys. Chem. B* **102**, 3586 (1998).

11. J. B. Lim, J. B. Klauda*, Biochim. Biophys. Acta* **1808**, 323 (2011).

12. J. Yoo, A. Aksimentiev, *J. Phys. Chem. Lett*. **3**, 45 (2012).

13. S. Miyamoto, P. A. Kollman, *J. Comput. Chem.* **13**, 952 (1992).

14. H. C. Andersen, *J. Comput. Phys.* **52**, 24 (1983).

15. P. F. Batcho, D. A. Case, T. Schlick, *J. Chem. Phys.* **115**, 4003 (2001).

16. R. D. Skeel, D. J. Hardy, J. C. Phillips, *J. Comput. Phys.* **225**, 1 (2007).

17. J. Yoo, A. Aksimentiev, *Proc. Natl. Acad. Sci. USA* **110**, 20099 (2013).

18. C. Maffeo, J. Yoo, A. Aksimentiev, De novo prediction of DNA origami structures through atomistic molecular dynamics simulation. *Nucleic Acids Res.,* accepted.

19. G. J. Martyna, D. J. Tobias, M. L. Klein, *J. Chem. Phys.* **101**, 4177 (1994).

20. S. E. Feller, Y. H. Zhang, R. W. Pastor, B. R. Brooks*, J. Chem. Phys.* **103**, 4613 (1995).

21. A. T. Brünger, X-PLOR, Version 3.1: A System for X-ray Crystallography and NMR, The Howard Hughes Medical Institute and Department of Molecular Biophysics and Biochemistry, Yale University (1992).

22. A. Aksimentiev, K. Schulten, *Biophys. J.* **88**, 3745 (2005).

23. A. Aksimentiev, J. B. Heng, G. Timp, K. Schulten, *Biophys. J.* **87**, 2086 (2004).

24. C. Y. Li, *et al., ACS Nano* **9**, 1420 (2015).

25. J. Yoo, A. Aksimentiev, *J. Phys. Chem. Lett.* **6**, 4680 (2015).

26. T. Thundat, D. P. Allison, R. J. Warmack, *Nucleic Acids Res.* **22**, 4224 (1994).

27. T. Nguyen, *et al., New J. Chem.* **38**, 5254 (2014).

28. K. Göpfrich, *et al., Nano Lett.* **15**, 3134 (2015).

29. S. Bhattacharya, J. Yoo, A. Aksimentiev, *ACS Nano* **10**, 4644 (2016).